5.1.3.7.2. *Reflection geometry*

In this case (Fig. 5.1.3.5) $S(\gamma_h)$ is now -1 and (5.1.3.10) may be written

$$\xi_j = S(C)\left[\eta \pm (\eta^2 - 1)^{1/2}\right]/|\gamma|^{1/2}. \qquad (5.1.3.12)$$

Now, let I_1 and I_2 be the points of the dispersion surface where the tangent is parallel to the normal to the crystal surface, and further let I_{o1}, I_{h1}, I' and I_{o2}, I_{h2}, I'' be the intersections of these two tangents with T_o, T_h and T'_o, respectively. For an incident wave of wavevector **OM** where M lies between I' and I'', the normal to the crystal surface drawn from M has no real intersection with the dispersion surface and $\overline{I'I''}$ defines the total-reflection domain. The tie points I_1 and I_2 correspond to $\eta = -1$ and $\eta = +1$, respectively, the extinction distance $\Lambda_L = 1/\overline{I_{o1}I_{h1}}$, the width of the total-reflection domain $2\delta = \overline{I_{o1}I_{o2}}/k = \overline{I'I''}/k$ and the deviation parameter $\eta = -\overline{M_oM_h}/\overline{I_{o1}I_{h1}}$, where M_o and M_h are the intersections with T_o and T_h of the normal to the crystal surface drawn from the extremity of any incident wavevector **OM**.

5.1.4. Standing waves

The various waves in a wavefield are coherent and interfere. In the two-beam case, the intensity of the wavefield, using (5.1.2.14) and (5.1.2.24), is

$$|D|^2 = |D_o|^2 \exp(4\pi \mathbf{K}_{oi} \cdot \mathbf{r}) \times [1 + |\xi|^2 + 2C|\xi| \cos 2\pi(\mathbf{h} \cdot \mathbf{r} + \Psi)], \qquad (5.1.4.1)$$

where Ψ is the phase of ξ,

$$\xi = |\xi| \exp(i\Psi). \qquad (5.1.4.2)$$

Equation (5.1.4.1) shows that the interference between the two waves is the origin of *standing waves*. The corresponding nodes lie on planes such that $\mathbf{h} \cdot \mathbf{r}$ is a constant. These planes are therefore parallel to the diffraction planes and their periodicity is equal to d_{hkl} (defined in the caption for Fig. 5.1.2.1*a*). Their position within the unit cell is given by the value of the phase Ψ.

In the Laue case, Ψ is equal to $\pi + \varphi_h$ for branch 1 and to φ_h for branch 2, where φ_h is the phase of the structure factor, (5.1.2.6). This means that the *nodes* of standing waves lie on the maxima of the *hkl* Fourier component of the electron density for branch 1 while the *anti-nodes* lie on the maxima for branch 2.

In the Bragg case, Ψ varies continuously from $\pi + \varphi_h$ to φ_h as the angle of incidence is varied from the low-angle side to the high-angle side of the reflection domain by rocking the crystal. The nodes lie on the maxima of the *hkl* Fourier components of the electron density on the low-angle side of the rocking curve. As the crystal is rocked, they are progressively shifted by half a lattice spacing until the anti-nodes lie on the maxima of the electron density on the high-angle side of the rocking curve.

Standing waves are the origin of the phenomenon of anomalous absorption, which is one of the specific properties of wavefields (Section 5.1.5). Anomalous scattering is also used for the location of atoms in the unit cell at the vicinity of the crystal surface: when X-rays are absorbed, fluorescent radiation and photoelectrons are emitted. Detection of this emission for a known angular position of the crystal with respect to the rocking curve and therefore for a known value of the phase Ψ enables the emitting atom within the unit cell to be located. The principle of this method is due to Batterman (1964, 1969). For reviews, see Golovchenko *et al.* (1982), Materlik & Zegenhagen (1984), Kovalchuk & Kohn (1986), Bedzyk (1988), Authier (1989), and Zegenhagen (1993).

5.1.5. Anomalous absorption

It was shown in Section 5.1.2.2 that the wavevectors of a given wavefield all have the same imaginary part (5.1.2.17) and therefore the same absorption coefficient μ (5.1.2.19). Borrmann (1950, 1954) showed that this coefficient is much smaller than the normal one (μ_o) for wavefields whose tie points lie on branch 1 of the dispersion surface and much larger for wavefields whose tie points lie on branch 2. The former case corresponds to the *anomalous transmission effect*, or *Borrmann effect*. As in favourable cases the minimum absorption coefficient may be as low as a few per cent of μ_o, this effect is very important from both a fundamental and a practical point of view.

The physical interpretation of the Borrmann effect is to be found in the standing waves described in Section 5.1.4. When the nodes of the electric field lie on the planes corresponding to the maxima of the *hkl* component of the electron density, the wavefields are absorbed anomalously less than when there is no diffraction. Just the opposite occurs for branch 2 wavefields, whose anti-nodes lie on the maxima of the electron density and which are absorbed more than normal.

The effective absorption coefficient μ is related to the imaginary part of the wavevectors through (5.1.2.19),

$$\mu = -4\pi\gamma_o K_{oi},$$

and to the imaginary part of the ratio of the amplitude of the reflected to the incident wave through

$$\mu = \mu_o - 4\pi X_{oi}, \qquad (5.1.5.1)$$

where X_{oi} is the imaginary part of X_o, which, using (5.1.2.24) and (5.1.3.10), is given by

$$X_o = R\lambda|C|S(\gamma_h)(F_hF_{\bar{h}})^{1/2} \times \{\eta \pm [\eta^2 + S(\gamma_h)]^{1/2}\}/\left[2\pi V(|\gamma|)^{1/2}\right]. \qquad (5.1.5.2)$$

Taking the upper sign (+) for the $\pm$ term corresponds to tie points on branch 1 and taking the lower sign $(-)$ corresponds to tie points on branch 2.

The calculation of the imaginary part X_{oi} is different in the Laue and in the Bragg cases. In the former case, the imaginary part of $(\eta^2 + 1)^{1/2}$ is small and can be approximated while in the latter, the imaginary part of $(\eta^2 - 1)^{1/2}$ is large when the real part of the deviation parameter, η_r, lies between 1 and -1, and cannot be calculated using the same approximation.

5.1.6. Intensities of plane waves in transmission geometry

5.1.6.1. *Absorption coefficient*

In transmission geometry, the imaginary part of X_o is small and, using a first-order approximation for the expansion of $(\eta^2 + 1)^{1/2}$, (5.1.5.1) and (5.1.5.2), the effective absorption coefficient in the absorption case is

$$\mu_j = \mu_o\left[\tfrac{1}{2}(1 + \gamma^{-1}). \mp \frac{(\eta_r/2)(1 - \gamma^{-1}) + |C|(\gamma^{-1})^{1/2}|F_{ih}/F_{io}| \cos\varphi}{(\eta_r^2 + 1)^{1/2}}\right], \qquad (5.1.6.1)$$

where $\varphi = \varphi_{rh} - \varphi_{ih}$ is the phase difference between F_{rh} and F_{ih} [equation (5.1.2.10)], the upper sign $(-)$ for the $\mp$ term corresponds to branch 1 and the lower sign (+) corresponds to branch 2 of the dispersion surface. In the symmetric Laue case ($\gamma = 1$, reflecting planes normal to the crystal surface), equation (5.1.6.1) reduces to

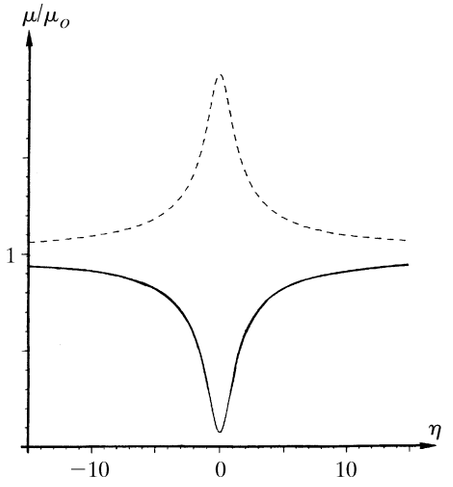

Fig. 5.1.6.1. Variation of the effective absorption with the deviation parameter in the transmission case for the 400 reflection of GaAs using Cu $K\alpha$ radiation. Solid curve: branch 1; broken curve: branch 2.

$$\mu_j = \mu_o \left[1 \mp \frac{|C||F_{ih}/F_{io}| \cos\varphi}{(\eta_r^2 + 1)^{1/2}} \right].$$

Fig. 5.1.6.1 shows the variations of the effective absorption coefficient μ_j with η_r for wavefields belonging to branches 1 and 2 in the case of the 400 reflection of GaAs with Cu $K\alpha$ radiation. It can be seen that for $\eta_r = 0$ the absorption coefficient for branch 1 becomes significantly smaller than the normal absorption coefficient, μ_o. The minimum absorption coefficient, $\mu_o(1 - |CF_{ih}/F_{io}| \cos\varphi)$, depends on the nature of the reflection through the structure factor and on the temperature through the Debye–Waller factor included in F_{ih} [equation (5.1.2.10*b*)] (Ohtsuki, 1964, 1965). For instance, in diamond-type structures, it is smaller for reflections with even indices than for reflections with odd indices. The influence of temperature is very important when $|F_{ih}/F_{io}|$ is close to one; for example, for germanium 220 and Mo $K\alpha$ radiation, the minimum absorption coefficient at 5 K is reduced to about 1% of its normal value, μ_o (Ludewig, 1969).

5.1.6.2. *Boundary conditions for the amplitudes at the entrance surface – intensities of the reflected and refracted waves*

Let us consider an infinite plane wave incident on a crystal plane surface of infinite lateral extension. As has been shown in Section 5.1.3, two wavefields are excited in the crystal, with tie points P_1 and P_2, and amplitudes D_{o1}, D_{h1} and D_{o2}, D_{h2}, respectively. Maxwell's boundary conditions (see Section A5.1.1.2 of the Appendix) imply continuity of the tangential component of the electric field and of the normal component of the electric displacement across the boundary. Because the index of refraction is so close to unity, one can assume to a very good approximation that there is continuity of the three components of both the electric field and the electric displacement. As a consequence, it can easily be shown that, *along the entrance surface*, for all components of the electric displacement

$$\begin{aligned} D_o^{(a)} &= D_{o1} + D_{o2} \\ 0 &= D_{h1} + D_{h2}, \end{aligned} \qquad (5.1.6.2)$$

where $D_o^{(a)}$ is the amplitude of the incident wave.

Using (5.1.3.11), (5.1.5.2) and (5.1.6.2), it can be shown that the *intensities* of the four waves are

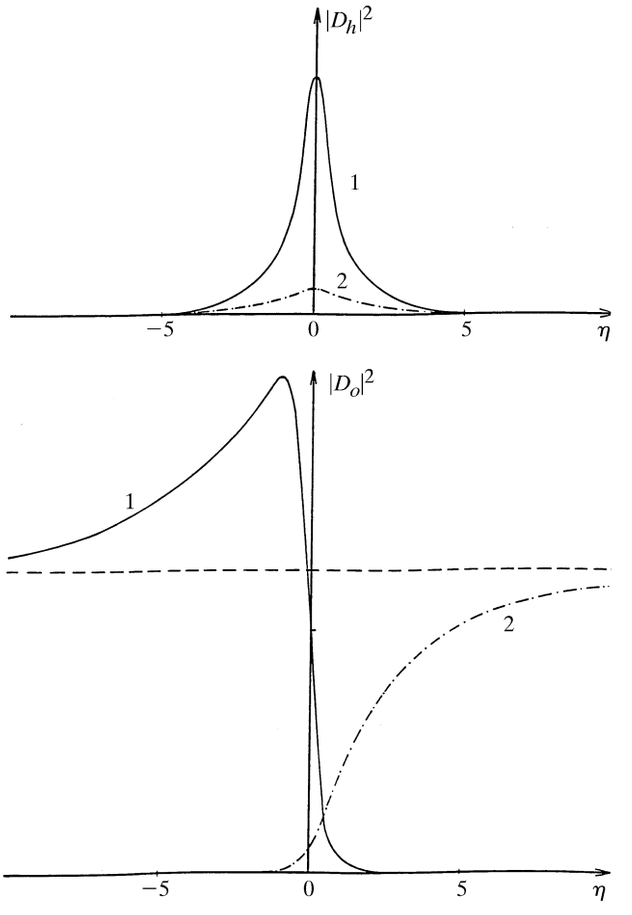

Fig. 5.1.6.2. Variation of the intensities of the reflected and refracted waves in an absorbing crystal for the 220 reflection of Si using Mo $K\alpha$ radiation, $t = 1$ mm ($\mu t = 1.42$). Solid curve: branch 1; dashed curve: branch 2.

$$\begin{aligned} |D_{oj}|^2 &= |D_o^{(a)}|^2 \exp(-\mu_j z/\gamma_o) \left[(1 + \eta_r^2)^{1/2} \mp \eta_r \right]^2 \\ &\quad \times [4(1 + \eta_r^2)]^{-1}, \\ |D_{hj}|^2 &= |D_o^{(a)}|^2 \exp(-\mu_j z/\gamma_o) |F_h/F_{\bar{h}}| [4\gamma(1 + \eta_r^2)]^{-1}; \end{aligned} \qquad (5.1.6.3)$$

top sign: $j = 1$; bottom sign: $j = 2$.

Fig. 5.1.6.2 represents the variations of these four intensities with the deviation parameter. Far from the reflection domain, $|D_{h1}|^2$ and $|D_{h2}|^2$ tend toward zero, as is normal, while

$$|D_{o1}|^2 \gg |D_{o2}|^2 \text{ for } \eta_r \Rightarrow -\infty,$$
$$|D_{o1}|^2 \ll |D_{o2}|^2 \text{ for } \eta_r \Rightarrow +\infty.$$

This result shows that the wavefield of highest intensity 'jumps' from one branch of the dispersion surface to the other across the reflection domain. This is an important property of dynamical theory which also holds in the Bragg case and when a wavefield crosses a highly distorted region in a deformed crystal [the so-called *interbranch scattering*: see, for instance, Authier & Balibar (1970) and Authier & Malgrange (1998)].

5.1.6.3. *Boundary conditions at the exit surface*

5.1.6.3.1. *Wavevectors*

When a wavefield reaches the exit surface, it breaks up into its two constituent waves. Their wavevectors are obtained by applying

again the condition of the continuity of their tangential components along the crystal surface. The extremities, M_j and N_j, of these wavevectors

$$\mathbf{OM}_j = \mathbf{K}_{\mathbf{o}j}^{(d)} \qquad \mathbf{HN}_j = \mathbf{K}_{\mathbf{h}j}^{(d)}$$

lie at the intersections of the spheres of radius k centred at O and H, respectively, with the normal $\mathbf{n}'$ to the crystal exit surface drawn from P_j ($j = 1$ and 2) (Fig. 5.1.6.3).

If the crystal is wedge-shaped and the normals $\mathbf{n}$ and $\mathbf{n}'$ to the entrance and exit surfaces are not parallel, the wavevectors of the waves generated by the two wavefields are not parallel. This effect is due to the refraction properties associated with the dispersion surface.

5.1.6.3.2. *Amplitudes – Pendellösung*

We shall assume from now on that the crystal is plane parallel. Two wavefields arrive at any point of the exit surface. Their constituent waves interfere and generate emerging waves in the refracted and reflected directions (Fig. 5.1.6.4). Their respective

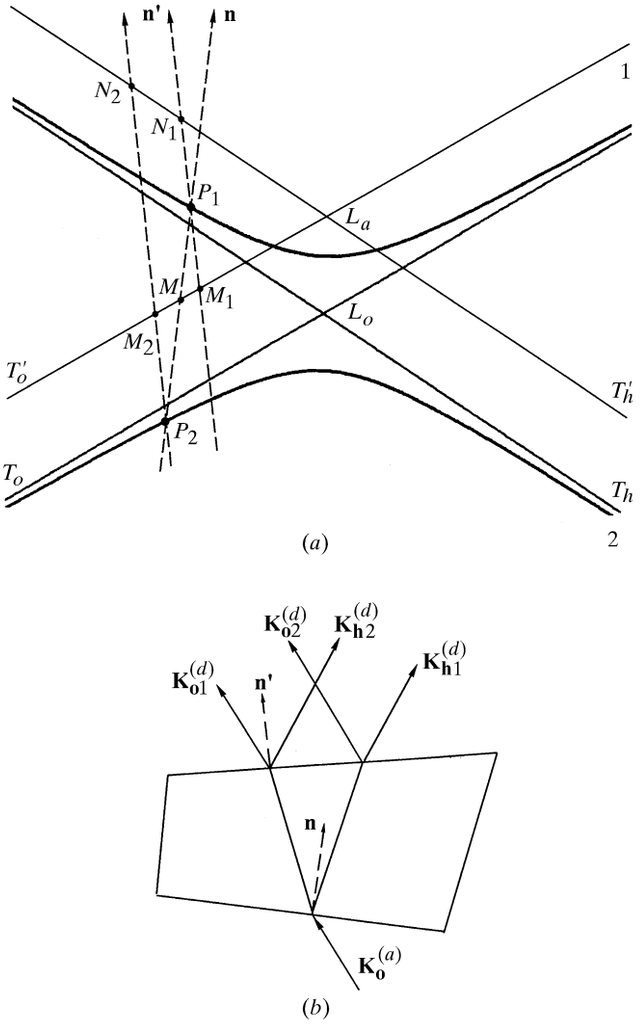

Fig. 5.1.6.3. Boundary condition for the wavevectors at the exit surface. (*a*) Reciprocal space. The wavevectors of the emerging waves are determined by the intersections M_1, M_2, N_1 and N_2 of the normals $\mathbf{n}'$ to the exit surface, drawn from the tie points P_1 and P_2 of the wavefields, with the tangents T'_o and T'_h to the spheres centred at O and H and of radius k, respectively. (*b*) Direct space.

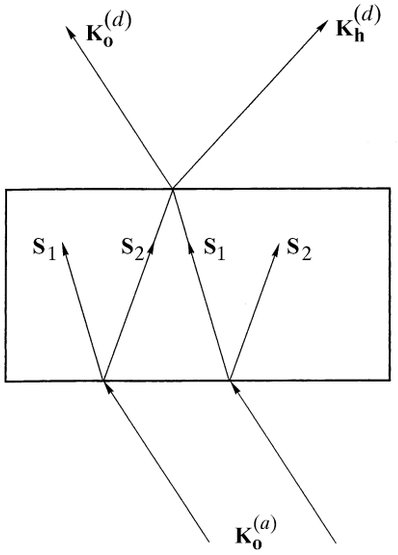

Fig. 5.1.6.4. Decomposition of a wavefield into its two components when it reaches the exit surface. $\mathbf{S}_1$ and $\mathbf{S}_2$ are the Poynting vectors of the two wavefields propagating in the crystal belonging to branches 1 and 2 of the dispersion surface, respectively, and interfering at the exit surface.

amplitudes are given by the boundary conditions

$$\begin{aligned} D_o^{(d)} \exp(-2\pi i \mathbf{K}_{\mathbf{o}}^{(d)} \cdot \mathbf{r}) &= D_{o1} \exp(-2\pi i \mathbf{K}_{\mathbf{o}1} \cdot \mathbf{r}) \\ &\quad + D_{o2} \exp(-2\pi i \mathbf{K}_{\mathbf{o}2} \cdot \mathbf{r}) \\ D_h^{(d)} \exp(-2\pi i \mathbf{K}_{\mathbf{h}}^{(d)} \cdot \mathbf{r}) &= D_{h1} \exp(-2\pi i \mathbf{K}_{\mathbf{h}1} \cdot \mathbf{r}) \\ &\quad + D_{h2} \exp(-2\pi i \mathbf{K}_{\mathbf{h}2} \cdot \mathbf{r}), \end{aligned} \tag{5.1.6.4}$$

where $\mathbf{r}$ is the position vector of a point on the exit surface, the origin of phases being taken at the entrance surface.

In a plane-parallel crystal, (5.1.6.4) reduces to

$$\begin{aligned} D_o^{(d)} &= D_{o1} \exp\big(-2\pi i \overline{MP_1} \cdot t\big) + D_{o2} \exp\big(-2\pi i \overline{MP_2} \cdot t\big) \\ D_h^{(d)} &= D_{h1} \exp\big(-2\pi i \overline{MP_1} \cdot t\big) + D_{h2} \exp\big(-2\pi i \overline{MP_2} \cdot t\big), \end{aligned}$$

where t is the crystal thickness.

In a *non-absorbing* crystal, the amplitudes squared are of the form

$$\big|D_o^{(d)}\big|^2 = |D_{o1}|^2 + |D_{o2}|^2 + 2D_{o1}D_{o2} \cos 2\pi \overline{P_2P_1} t.$$

This expression shows that the intensities of the refracted and reflected beams are oscillating functions of crystal thickness. The period of the oscillations is called the *Pendellösung* distance and is

$$\Lambda = 1/\overline{P_2P_1} = \Lambda_L/(1 + \eta_r^2)^{1/2}.$$

5.1.6.4. *Reflecting power*

For an *absorbing* crystal, the intensities of the reflected and refracted waves are

$$\begin{aligned} \big|D_o^{(d)}\big|^2 &= \big|D_o^{(a)}\big|^2 A_\eta \Big\{ \cosh(2v + \mu_a t). \\ &\qquad + \cos\Big[2\pi t \Lambda^{-1} - 2\eta_i (1 + \eta_r^2)^{-1/2}\Big] \Big\} \\ \Big|D_h^{(d)}\Big|^2 &= \big|D_o^{(a)}\big|^2 |F_h/F_{\bar{h}}| \gamma^{-1} A_\eta \big[\cosh(\mu_a t) - \cos(2\pi t \Lambda^{-1})\big], \end{aligned} \tag{5.1.6.5}$$

where

$$A_\eta = \left[\exp -\mu_o t(\gamma_o^{-1} + \gamma_h^{-1})\right]/2(1+\eta_r^2),$$
$$\mu_a = \mu_j\Big[1/2(\gamma_o^{-1} - \gamma_h^{-1})\eta_r + |C||F_{ih}/F_{io}|\cos\varphi/(\gamma_o\gamma_h)^{1/2}\Big](1+\eta_r^2)^{-1/2},$$
$$v = \operatorname{arg\,sinh}\eta_r$$

and μ_j is given by equation (5.1.6.1).

Depending on the absorption coefficient, the cosine terms are more or less important relative to the hyperbolic cosine term and the oscillations due to *Pendellösung* have more or less contrast.

For a non-absorbing crystal, these expressions reduce to

$$\left|D_o^{(d)}\right|^2 = \left|D_o^{(a)}\right|^2\left[\frac{1+2\eta^2+\cos(2\pi t\Lambda^{-1})}{2(1+\eta_r^2)}\right],$$
$$\left|D_h^{(d)}\right|^2 = \left|D_o^{(a)}\right|^2\left[\frac{1-\cos(2\pi t\Lambda^{-1})}{2\gamma(1+\eta_r^2)}\right]. \qquad (5.1.6.6)$$

What is actually measured in a counter receiving the reflected or the refracted beam is the *reflecting power*, namely the ratio of the energy of the reflected or refracted beam on the one hand and the energy of the incident beam on the other. The energy of a beam is obtained by multiplying its intensity by its cross section. If l is the width of the trace of the beam on the crystal surface, the cross sections of the incident (or refracted) and reflected beams are proportional to (Fig. 5.1.6.5) $l_o = l\gamma_o$ and $l_h = l\gamma_h$, respectively.

The reflecting powers are therefore:

$$\text{Refracted beam: } I_o = l_o\left|D_o^{(d)}\right|^2\Big/ l_o\left|D_o^{(a)}\right|^2 = \left|D_o^{(d)}\right|^2\Big/\left|D_o^{(a)}\right|^2,$$
$$\text{Reflected beam: } I_h = l_h\left|D_h^{(d)}\right|^2\Big/ l_o\left|D_o^{(a)}\right|^2 = \gamma\left|D_h^{(d)}\right|^2\Big/\left|D_o^{(a)}\right|^2. \qquad (5.1.6.7)$$

Using (5.1.6.6), it is easy to check that $I_o + I_h = 1$ in the non-absorbing case; that is, that conservation of energy is satisfied. Equations (5.1.6.6) show that there is a periodic exchange of energy between the refracted and the reflected waves as the beam penetrates the crystal; this is why Ewald introduced the expression *Pendellösung*.

The oscillations in the rocking curve were first observed by Lefeld-Sosnowska & Malgrange (1968, 1969). Their periodicity can be used for accurate measurements of the form factor [see, for instance, Bonse & Teworte (1980)]. Fig. 5.1.6.6 shows the shape of the rocking curve for various values of t/Λ_L.

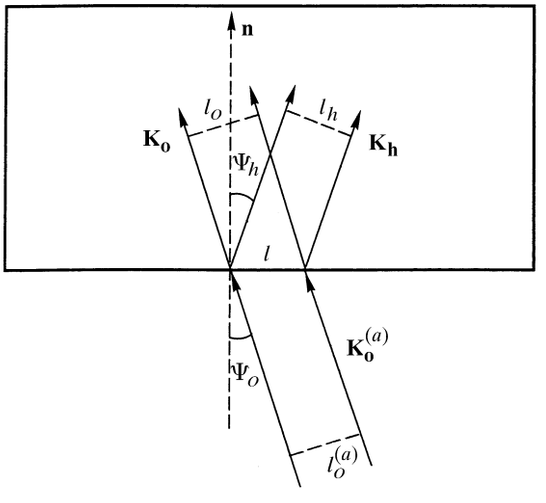

Fig. 5.1.6.5. Cross sections of the incident, $\mathbf{K}_\mathbf{o}^{(a)}$, refracted, $\mathbf{K_o}$, and reflected, $\mathbf{K_h}$, waves.

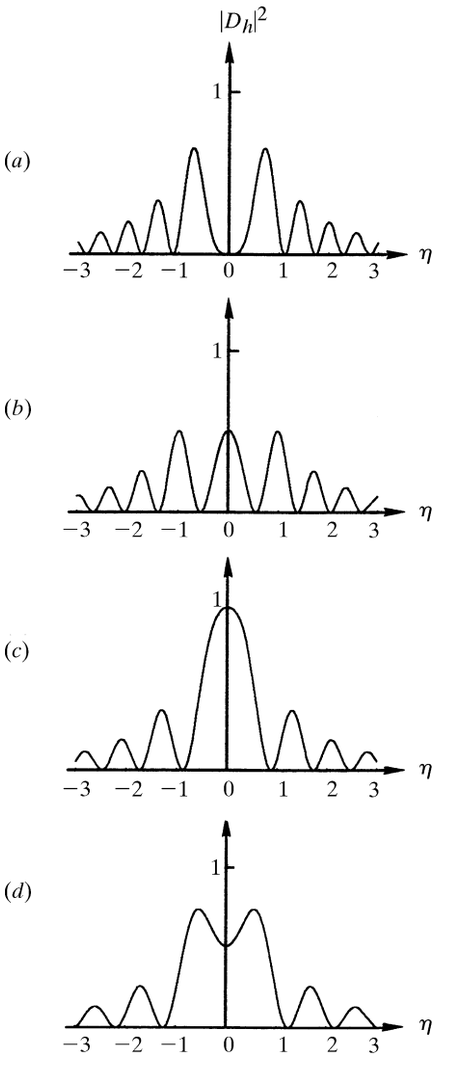

Fig. 5.1.6.6. Theoretical rocking curves in the transmission case for non-absorbing crystals and for various values of t/Λ_L: (*a*) $t/\Lambda_L = 1.25$; (*b*) $t/\Lambda_L = 1.5$; (*c*) $t/\Lambda_L = 1.75$; (*d*) $t/\Lambda_L = 2.0$.

The *width at half-height of the rocking curve*, averaged over the *Pendellösung* oscillations, corresponds in the non-absorbing case to $\Delta\eta = 2$, that is, to $\Delta\theta = 2\delta$, where δ is given by (5.1.3.6).

5.1.6.5. *Integrated intensity*

5.1.6.5.1. *Non-absorbing crystals*

The integrated intensity is the ratio of the total energy recorded in the counter when the crystal is rocked to the intensity of the incident beam. It is proportional to the area under the line profile:

$$I_{hi} = \int_{-\infty}^{+\infty} I_h\, \mathrm{d}(\Delta\theta). \qquad (5.1.6.8)$$

The integration was performed by von Laue (1960). Using (5.1.3.5), (5.1.6.6) and (5.1.6.7) gives

$$I_{hi} = A\int_0^{2\pi t\Lambda_L^{-1}} J_0(z)\, \mathrm{d}z,$$

where $J_0(z)$ is the zeroth-order Bessel function and

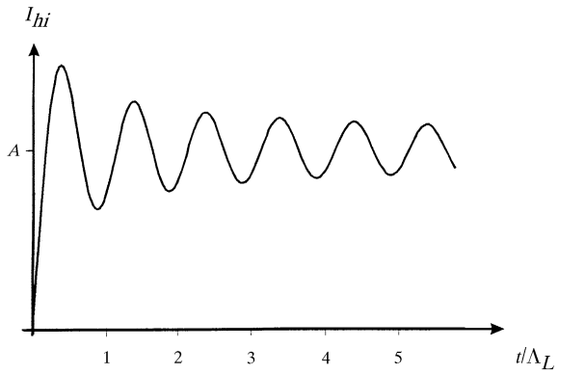

Fig. 5.1.6.7. Variations with crystal thickness of the integrated intensity in the transmission case (no absorption) (arbitrary units). The expression for A is given in the text.

$$A = \frac{R\lambda^2|CF_h|(\gamma)^{1/2}}{2V\sin 2\theta}.$$

Fig. 5.1.6.7 shows the variations of the integrated intensity with t/Λ_L.

5.1.6.5.2. *Absorbing crystals*

The integration was performed for absorbing crystals by Kato (1955). The integrated intensity in this case is given by

$$I_{hi} = A|F_h/F_{\bar{h}}|\exp\left[-1/2\mu_o t(\gamma_o^{-1}+\gamma_h^{-1})\right] \times \left[\int_0^{2\pi t\Lambda_L^{-1}} J_0(z)\,\mathrm{d}z - 1 + I_0(\zeta)\right],$$

where

$$\zeta = \mu_o t\left\{\left[|C|^2|F_{ih}/F_{io}|^2\cos^2\varphi + (\gamma_h-\gamma_o)/(4\gamma_o\gamma_h)\right]/(\gamma_o\gamma_h)\right\}^{1/2}$$

and $I_0(\zeta)$ is a modified Bessel function of zeroth order.

5.1.6.6. *Thin crystals – comparison with geometrical theory*

Using (5.1.6.6) and (5.1.6.7), the reflecting power of the reflected beam may also be written

$$I_h = \pi^2 t^2 \Lambda_o^{-2} f(\eta),$$

where

$$f(\eta) = \left[\frac{\sin U(1+\eta^2)^{1/2}}{U(1+\eta^2)^{1/2}}\right]^2$$

and

$$U = \pi t\Lambda_o^{-1}.$$

When $t\Lambda_o^{-1}$ is very small, $f(\eta)$ tends asymptotically towards the function

$$f_1(\eta) = \left[\frac{\sin U\eta}{U\eta}\right]^2$$

and I_h towards the value given by geometrical theory. The condition for geometrical theory to apply is, therefore, that the crystal thickness be much smaller than the *Pendellösung* distance. In practice, the two theories agree to within a few per cent for a crystal thickness smaller than or equal to a third of the *Pendellösung* distance [see Authier & Malgrange (1998)].

5.1.7. Intensity of plane waves in reflection geometry

5.1.7.1. *Thick crystals*

5.1.7.1.1. *Non-absorbing crystals*

Rocking curve. The geometrical construction in Fig. 5.1.3.5 shows that, in the Bragg case, the normal to the crystal surface drawn from the extremity of the incident wavevector intersects the dispersion surface either at two points of the same branch, P_1, P_1', for branch 1, P_2, P_2' for branch 2, or at imaginary points. It was shown in Section 5.1.2.6 that the propagation of the wavefields inside the crystal is along the normal to the dispersion surface at the corresponding tie points. Fig. 5.1.3.5 shows that this direction is oriented towards the outside of the crystal for tie points P_1' and P_2'. In a very thick crystal, these wavefields cannot exist because there is always a small amount of absorption. One concludes that in the thick-crystal case and in reflection geometry, only one wavefield is excited inside the crystal. It corresponds to branch 1 on the low-angle side of the rocking curve and to branch 2 on the high-angle side. Using the same approximations as in Section 5.1.6.2, the amplitude $\mathbf{D}_\mathbf{h}^{(a)}$ of the wave reflected at the crystal surface is obtained by applying the boundary conditions, which are particularly simple in this case:

$$\mathbf{D_o} = \mathbf{D_o}^{(a)},\ \mathbf{D_h}^{(a)} = \mathbf{D_h}.$$

The reflecting power is given by an expression similar to (5.1.6.7):

$$I_h = |\gamma||\xi_j|^2,$$

where the expression for ξ_j is given by (5.1.3.12), and $j = 1$ or 2 depending on which wavefield propagates towards the inside of the crystal. When the normal to the entrance surface intersects the dispersion surface at imaginary points, *i.e.* when $-1 < \eta < +1$,

$$|\xi|^2 = |\gamma|^{-1},\ I_h = 1, \qquad (5.1.7.1)$$

and there is *total reflection.* Outside the total-reflection domain, the reflecting power is given by

$$I_h = \left[|\eta| - (\eta^2-1)^{1/2}\right]^2. \qquad (5.1.7.2)$$

The rocking curve has the well known top-hat shape (Fig. 5.1.7.1). Far from the total-reflection domain, the curve can be

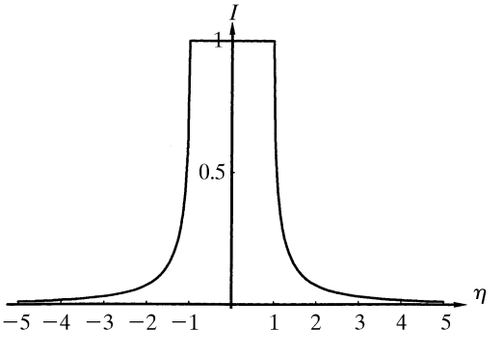

Fig. 5.1.7.1. Theoretical rocking curve in the reflection case for a non-absorbing thick crystal in terms of the deviation parameter.

references